

Contents lists available at ScienceDirect

# Physica B: Condensed Matter

journal homepage: www.elsevier.com/locate/physb





# Influence of Sr doping on the structural and magnetic properties of $(Y,Gd)Ba_{1-x}Sr_xCuFeO_5$ (x=0,0.25,0.5) studied by FTIR and <sup>57</sup>Fe Mössbauer spectroscopy

I.M. Saavedra-Gaona <sup>a</sup>, F. Mesquita <sup>b</sup>, R. Cohen <sup>c</sup>, L.C.C.M. Nagamine <sup>c</sup>, C.A. Parra-Vargas <sup>a</sup>, J. Munevar <sup>d,\*</sup>

- a Grupo Fisica de Materiales, Escuela de Fisica, Universidad Pedagogica y Tecnologica de Colombia, Avenida Central del Norte 39-115, Tunja, 150003, Colombia
- <sup>b</sup> Departamento de Fisica, Universidade Federal do Rio Grande do Sul, Porto Alegre RS, Brazil
- c Instituto de Fisica, Universidade de Sao Paulo, Sao Paulo SP, Brazil
- d CCNH, Universidade Federal do ABC (UFABC), 09210-580, Santo Andre, SP, Brazil

#### ARTICLE INFO

#### Keywords: Perovskites Multiferroics Mössbauer spectroscopy Antiferromagnetism

#### ABSTRACT

The effect of replacing Y by Gd and Ba by Sr in YBaCuFeO $_5$  is studied by Fourier Transform Infrared spectroscopy,  $^{57}$ Fe Mössbauer spectroscopy and DC susceptibility measurements. Site disorder is inferred from FTIR and Mössbauer spectra using a Maximum-Entropy-Method. A doping dependence of the IR peaks and the hyperfine parameters is explained in terms of bonding energies and electric field gradient variations in the crystal lattice caused by Fe/Cu site disorder. We find an influence of doping on the structural and magnetic properties through a correlation of hyperfine parameters such as the electric quadrupole splitting and the magnetic hyperfine field. We also find that a paramagnetic volume fraction appears for GdBaCuFeO $_5$  that increases upon Sr doping at the Ba site. The different behavior of the susceptibility upon replacing Y by Gd is attributed to the lack of a favorable environment to enable a Gd-Fe or Gd-Cu exchange interaction.

# 1. Introduction

Multiferroics are materials where ferroelectric and (ferro)magnetic orders are present, and the potential coupling between these orders makes these materials interesting for technological applications [1,2]. BiFeO<sub>3</sub> is probably one of the most famous examples of multiferroics, where the ferroelectricity is caused by a Bi  $6s^2$  lone pair that creates a charge imbalance in the unit cell leading to an electric polarization, and the magnetic order is caused by exchange interactions between Fe moments [3]. TbMnO<sub>3</sub> is another remarkable example of multiferroics, though it belongs to another type of multiferroics where ferroelectric and magnetic order are correlated; usually the onset of a spiral magnetic state is accompanied by the observation of a robust electric polarization [4]. Magnetically frustrated YBaCuFeO<sub>5</sub> is a material that can potentially host multiferroicity at room temperature, and hence its interest [5–13]. Its crystal structure is composed by bipyramids formed by Fe/Cu atoms in the base of the pyramids and O atoms in their vertices, in which between these bipyramids are located Ba atoms, and Y atoms are located between the bipyramid layers [6,11,14,15]. The crystal symmetry is tetragonal with space group P4 mm confirmed by detailed X-ray and neutron diffraction [6,7,11,16,17], and Raman and

Fourier transform infrared (FTIR) spectroscopies [18]. The crystal structure is shown in Fig. 1. YBaCuFeO $_5$  shows two magnetic transitions; one from paramagnetic to collinear antiferromagnetic (AFM) order at approximately  $T_{N1} \simeq 450$  K, and another from the collinear AFM to a spiral AFM state at approximately  $T_{N2} \simeq 200$  K [14–16]. Ferroelectric response and large dielectric constant below  $T_{N2}$  has been reported for YBaCuFeO $_5$  as well [5,6,8,9,19], which suggest this compound may have a multiferroic nature. <sup>57</sup>Fe Mössbauer studies have revealed a broadened sextet at room temperature [14–16,20], due to the onset of collinear AFM order combined with inequivalent Fe sites observed in the paramagnetic phase [16], and the resonance line broadening persists at low temperatures.

Further interest has arisen around YBaCuFeO $_5$  after it was demonstrated that is one of the few examples where spiral order is enhanced by Fe/Cu site disorder [6,7,11,17,21,22]. This site disorder has allowed the increase of  $T_{N2}$  up to values above room temperature. A strong correlation between site disorder, magnetic incommensurability and the increase of  $T_{N2}$  is explained by the different magnetic exchange interactions that can arise between neighboring Fe/Cu moments. In the perfectly ordered structure, *i.e.* bipyramids formed by Fe and Cu

<sup>\*</sup> Correspondence to: CCNH, Universidade Federal do ABC (UFABC), Avenida dos Estados, 5001 – Bairro Bangu – Santo Andre/SP – CEP 09280-560, Brazil. E-mail address: julian.munevar@ufabc.edu.br (J. Munevar).

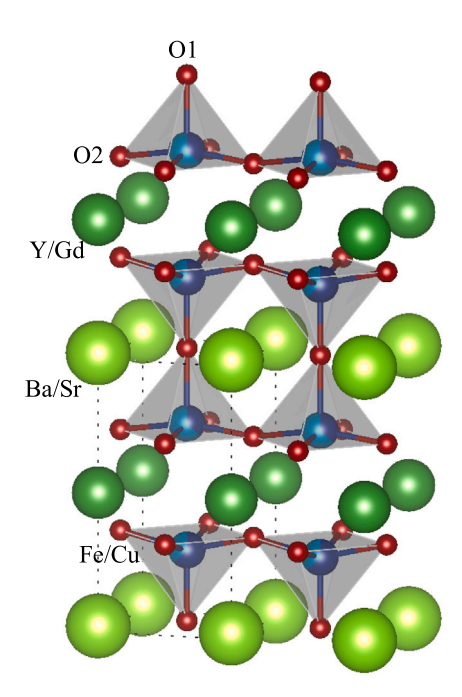


Fig. 1. Crystal structure of YBaCuFeO $_5$  [14]. Dark green spheres represent Y/Gd atoms, light green spheres represent Ba/Sr atoms, Fe/Cu atoms are represented with light blue/dark blue spheres, and oxygen is represented with red spheres. The Fe/Cu bipyramids are also shown.

pyramids throughout the crystal, AFM interactions in the ab plane as well as along the c axis leading to a collinear AFM order are expected; if site disorder is present, Fe–Fe and Cu–Cu pairs begin to form, and the Fe–Fe bipyramids are considered as responsible for the onset of the spiral state [6,11,21,22].

One possibility to control the Fe/Cu site disorder is tuning it by control of the sintering conditions; the faster the cooling conditions after heat treatment, the larger the site disorder [6,11,17]. This enhanced site disorder is accompanied with a larger incommensurability of the spiral wave vector ( $\mathbf{k} = (1/2, 1/2, 1/2 + q)$ ) where q is the magnetic modulation parameter) below  $T_{N2}$  and with the size and separation between bipyramids in the crystal structure. This sensitivity to small perturbations in the crystal structure can be also exploited by replacing Ba by Ca and Sr [7,11,23-25], or by replacing Y by rare earth elements [11,20,26,27].  $T_{N2}$  has been increased up to 300 K for DyBaCuFeO5, which is above room temperature and stands as a promising material for technological applications [11]. Also recently, the structural analysis previously reported for the samples used in this study suggests that the effect of increasing the ionic radius at the Y and Ba sites leads to the increase of key parameters such as the tetragonal distortion c/2a, the ratio between the bipyramid separating layer distance  $d_2$  and the bipyramid height  $d_1$ , and the Fe–O and Cu–O

Providing a local view of the Fe/Cu site disorder and the influence of cation substitutions will be important to understand further the underlying mechanisms in the formation of the spiral structure below  $T_{N2}$  and their relation to the magnetic ground state. In this manuscript, we report FTIR,  $^{57}$ Fe Mössbauer and magnetization measurements on  $(Y,Gd)Ba_{1-x}Sr_xCuFeO_5$ , and the results found give insight on the role of local disorder induced by doping in different crystallographic sites on the macroscopic and local magnetic response.

#### 2. Materials and methods

Single phase polycrystalline samples of  $YBa_{1-x}Sr_xCuFeO_5$  and  $GdBa_{1-x}Sr_xCuFeO_5$  (x=0,0.25,0.5) previously grown by the solid-state

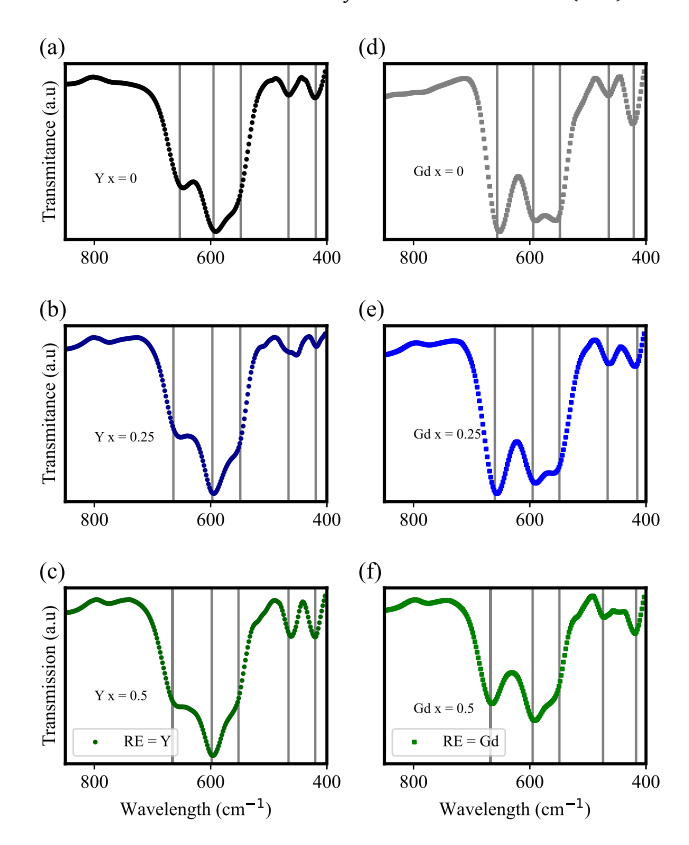


**Fig. 2.** FTIR spectra for  $YBa_{1-x}Sr_xCuFeO_5$  (panels on the left (a-c)) and  $GdBa_{1-x}Sr_xCuFeO_5$  (panels on the right (d-f)) between 900–400 cm<sup>-1</sup>. The data points are shown in blue for  $YBa_{1-x}Sr_xCuFeO_5$  and gray for  $GdBa_{1-x}Sr_xCuFeO_5$ , and the vertical lines indicate the position of the bands.

reaction method has been used for this study [28]. Fourier transform infrared (FTIR) spectroscopy experiments have been obtained at room temperature using a IRPrestige-21 Shimadzu spectrophotometer equipped with a diamond crystal cell for the total attenuated reflection mode. The spectra were acquired by 8 scans per sample in the 4500 – 400 nm range, and the spectral resolution was set to 8 cm<sup>-1</sup>. <sup>57</sup>Fe Mössbauer spectra were measured in a standard Mössbauer spectrometer in the transmission mode using a <sup>57</sup>Co:Rh source moving in a constant velocity mode, and the measurements were performed at 80 K and 300 K using a liquid nitrogen cryostat. The analysis of the Mössbauer spectra was performed by using the Moessfit software package [29], which allows fitting models using magnetic hyperfine field distributions calculated by the maximum entropy method (MEM) and correlation between hyperfine parameters. Temperature-dependent DC magnetization measurements were performed in a QuantumDesign Physical Property Measurement System (PPMS) using the vibrating sample mode (VSM) option, with temperatures ranging between 2 and 380 K and applied fields of 1 kOe.

#### 3. Results

#### 3.1. FTIR

Fig. 2 shows the FTIR spectra measured for  $YBa_{1-x}Sr_xCuFeO_5$  (a-c) and  $GdBa_{1-x}Sr_xCuFeO_5$  (d-f) in the 900–400 cm<sup>-1</sup> range, with three strong and few weak bands, typical of perovskite layered compounds [18,30]. Since the bands are somewhat broadened, the second derivative of the IR transmission was calculated in order to facilitate the extraction of the positions of the corresponding bands. The three strong bands are positioned at 666.1–655.4 cm<sup>-1</sup> (strong  $v_1$ ), 596.3–591.2 cm<sup>-1</sup> (strong  $v_2$ ) and 554.5–541.7 cm<sup>-1</sup> (strong  $v_3$ ), associated

Table 1 Peak positions extracted from FTIR spectra measured for  $YBa_{1-x}Sr_xCuFeO_5$ .

Sample	$\mathbf{Y} \ x = 0$	Y x = 0.25	Y $x = 0.5$
$\nu_1$	653(2)	664(1)	666(2)
$\nu_2$	595(1)	597(1)	598(1)
$\nu_3$	548(2)	549(1)	552(1)
$\nu_4$	466(4)	466(4)	466(3)
$v_5$	419(4)	419(3)	420(3)

 $\begin{tabular}{lll} \textbf{Table 2} \\ \textbf{Peak positions extracted from FTIR spectra measured for } \\ \textbf{GdBa}_{1-x}\textbf{Sr}_x\textbf{CuFeO}_5. \\ \end{tabular}$ 

Sample	Gd x = 0	Gd $x = 0.25$	Gd $x = 0.5$
$\nu_1$	656(2)	660(1)	667(2)
$\nu_2$	594(1)	595(1)	595(1)
$\nu_3$	548(2)	549(1)	549(1)
$\nu_4$	464(4)	466(4)	474(3)
$\nu_5$	421(4)	415(3)	417(3)

to the vibration of apical O1 atoms in the 1*b* Wyckoff position  $(v_1)$ , and stretching of Cu-O2-Fe bonds in basal planes with O2 in the 2*c* Wyckoff position  $(v_2$  and  $v_3)$ , respectively [18]. A variation of the relative intensities of the  $v_1$ - $v_3$  bands after replacing Y by Gd and by replacing Ba by Sr in YBaCuFeO<sub>5</sub> is also noticed. The weak bands observed are located at 469.1–460.2 cm<sup>-1</sup> (weak  $v_4$ ) are associated to Cu-O2-Fe vibrations, and bands located at 419.1–416.6 cm<sup>-1</sup> (weak  $v_5$ ) are probably related to impurities or site defects. These results are reported in Tables 1 and 2.

The displacements of the  $v_1$  band towards higher values show that the vibrations of the apical oxygen are very sensitive to variations of the Sr content at the Ba site. Since the Ba site (1a Wyckoff position) is in between the bipyramids, it is therefore expected that a smaller ionic radius leads to smaller Cu/Fe-O distances, a larger bonding energy and hence an increase in the wavenumber. The effect of Gd substitution at the Y site (1a Wyckoff position) leads to an increase in ionic radius, leading to a reduction of Cu/Fe-O distances, larger bonding energies and to a further increase in the  $v_1$  peak wavenumber. On the other hand, the  $v_2$  and  $v_3$  bands, related to the basal vibrations of the Cu-O2-Fe bonds, show a very small variation upon Sr doping, reflecting little effect to the in-plane atomic bonds and distances [31].

Regarding the peak widths, only  $\nu_2$  shows a consistent variation from 43(4) cm<sup>-1</sup> to 63(4) cm<sup>-1</sup> for the YBa<sub>1-x</sub>Sr<sub>x</sub>CuFeO<sub>5</sub>, and from 52(10) cm<sup>-1</sup> to 58(4) cm<sup>-1</sup> for the GdBa<sub>1-x</sub>Sr<sub>x</sub>CuFeO<sub>5</sub>. This can be understood by considering enhanced site disorder at the Fe/Cu sites by doping [32]. This enhanced disorder seen in the basal Cu-O-Fe planes will be connected to the magnetic behavior below.

### 3.2. Mössbauer spectroscopy

The  $^{57}$ Fe Mössbauer spectra measured for the YBa $_{1-x}$ Sr $_x$ CuFeO $_5$  at 80 and 300 K are shown in Fig. 3(a)–(f), and the spectra for the GdBa $_{1-x}$ Sr $_x$ CuFeO $_5$  are shown in Fig. 4(a)–(f). A sextet with broad lines is observed for all the spectra, which confirm their magnetically ordered nature in the measured temperatures. The GdBa $_{1-x}$ Sr $_x$ CuFeO $_5$  spectra also show a paramagnetic doublet, which will be discussed below.

Due to the line broadening observed in the spectra, a model using a distribution of hyperfine fields is used. Nevertheless, a standard histogram model for the magnetic hyperfine field was tested without a satisfactory fit. One of the possible causes of the line broadening is the presence of inequivalent Fe sites due to their local environment, *i.e.* the influence of neighboring atoms on the Fe site, which is strongly dependent on the growth conditions [6,11,16,17]. Previous Mössbauer studies on YBaCuFeO<sub>5</sub> [14,16] and LaBaFe<sub>0.5</sub>Ti<sub>0.5</sub>MnO<sub>6- $\delta$ </sub> [33] have

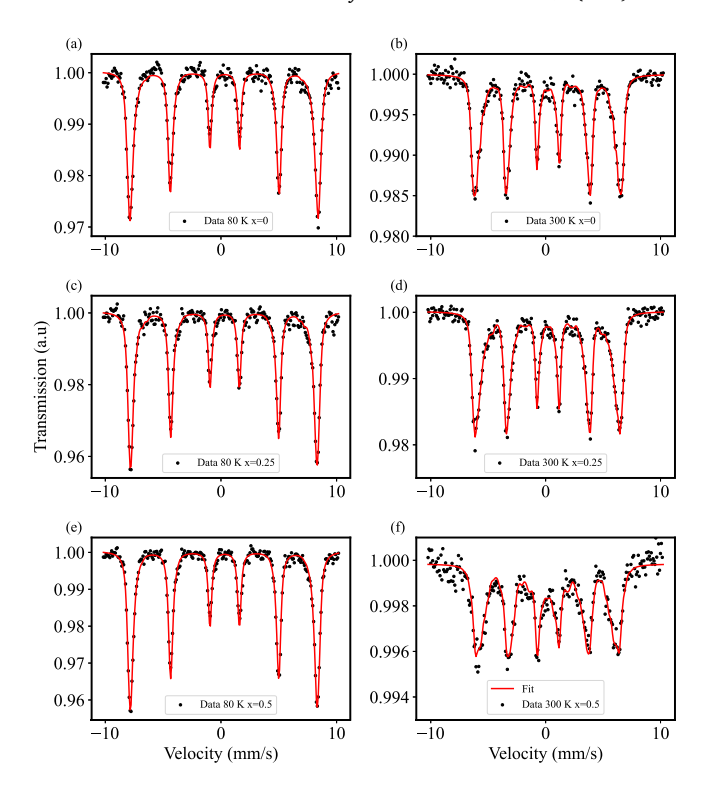


**Fig. 3.** Mössbauer spectra for YBa $_{1-x}$ Sr $_x$ CuFeO $_5$  x=0 at measured at 80 K (a) and 300 K (b), x=0.25 at 80 K (c) and 300 K (d), and x=0.5 at 80 K (e) and 300 K (f). Experimental data is represented by black dots, blue lines represent the fitted doublets, green lines represent magnetic distribution and total fits are represented by red lines.

suggested that in the presence of site disorder at the Fe site, a distribution of quadrupole splitting values  $\Delta E_Q$  should be expected, accounting for the different local electric field gradient interactions for every set of atoms in each configuration, as it was observed in the paramagnetic state for YBaCuFeO\_5[16]. In addition, the role of different Fe–Fe, Fe–Cu and Cu–Cu magnetic exchange interactions, as has been explained [21, 22], lead to different local Fe environments, hence different magnetic hyperfine fields should be expected. For this reason, our approach involves a hyperfine field distribution calculated using the Maximum Entropy Method (MEM) [29], modeling the site inhomogeneities with a linear dependence of the quadrupole splitting and the hyperfine magnetic field. An equivalent approach would be the use of more than one Fe sextet [14–16,20], however, it would be necessary to impose constraints between the parameters to obtain meaningful results.

The above proposed model brings two challenges to this work: 1. the Mössbauer spectra presented in this study were obtained below  $T_{N1}$  which implies to take into account electric and magnetic interactions simultaneously, and 2. the Mössbauer spectra at room temperature may be in the spiral state if  $T_{N2}$  is above room temperature. These challenges can be tackled by using a distribution of  $B_{hf}$  and a correlation between  $\Delta E_Q$  and the magnetic hyperfine field  $B_{hf}$ , which improved the quality of the fits, in particular those regions close to the base of the resonance lines, where a standard  $B_{hf}$  distribution was not sufficient to obtain good fits.

This MEM method was used within the Full Hamiltonian site model for the hyperfine parameters at the Fe sites. The fitted parameters were the spectral area A, the isomer shift  $\delta$ , the linewidth  $\Gamma$ , the magnetic hyperfine field  $B_{hf}$ , the quadrupole splitting  $\Delta E_Q$ , the correlation parameters between  $B_{hf}$  and  $\Delta E_Q$  defined as a and b, and the angle  $\theta$  between  $B_{hf}$  and the electric field gradient main component  $V_{zz}$ , the latter assumed to be parallel to the crystallographic c axis. For comparison with the available data in the literature, we estimated the quadrupole lineshift  $2\varepsilon$  from  $\Delta E_Q$  and  $\theta$ . For the GdBa $_{1-x}$ Sr $_x$ CuFeO $_5$ 

Table 3
Hyperfine parameters extracted from the fits shown in Figs. 3 and 4 for YBa<sub>1-x</sub>Sr<sub>x</sub>CuFeO<sub>5</sub> and GdBa<sub>1-x</sub>Sr<sub>x</sub>CuFeO<sub>5</sub>.

×1 1				•	1-X X	-	1 4 4 5	
Sample	T (K)	$\delta$ (mm/s)	$\overline{\Delta E_Q}$ (mm/s)	$\overline{B_{hf}}$ ()	θ (°)	$2\varepsilon$ (mm/s)	Γ (mm/s)	A (%)
$\mathbf{Y} \ x = 0$	300	0.306(7)	0.35(10)	36(7)	61.3(5)	-0.05(2)	0.28(1)	100
	80	0.405(3)	0.13(2)	50.1(1.9)	88.3(7)	-0.06(1)	0.32(1)	100
Y x = 0.25	300	0.299(8)	0.24(12)	35(7)	69.6(5)	-0.08(4)	0.28(1)	100
	80	0.394(3)	0.16(3)	49.5(1.9)	87.6(7)	-0.08(1)	0.32(1)	100
Y x = 0.5	300	0.285(20)	0.29(17)	32(10)	74.4(5)	-0.11(7)	0.42(1)	100
	80	0.394(3)	0.23(2)	49.9(1.4)	71.7(8)	-0.08(1)	0.35(1)	100
Gd x = 0	300	0.303(12)	0.12(9)	33(6)	67.6(8)	-0.03(2)	0.30(1)	88(1)
	300	0.239(2)	0.25(2)	_	-	-	-	12(1)
	80	0.508(6)	0.25(2)	49.9(1.8)	75.0(5)	-0.10(1)	0.30(1)	92(1)
	80	0.327(2)	0.34(2)	_	_	_	_	8(2)
Gd $x = 0.25$	300	0.286(2)	0.27(12)	32(8)	70.78(9)	-0.09(4)	0.36(1)	91(1)
	300	0.222(2)	0.25(5)	_	_	_	_	9(1)
	80	0.500(4)	0.25(2)	49.1(1.6)	79.5(7)	-0.11(1)	0.30(1)	96(1)
	80	0.394(2)	0.34(2)	_	_	_	_	4(2)
Gd $x = 0.5$	300	0.27	0.31(16)	31(9)	76.6(10)	-0.13(7)	0.34(1)	83(1)
	300	0.229(2)	0.25(5)	-	_	_	_	17(1)
	80	0.502(4)	0.31(2)	50.1(1.9)	72.08(7)	-0.11(1)	0.30(1)	92(1)
	80	0.399(1)	0.37(5)	-	-	-	-	8(2)

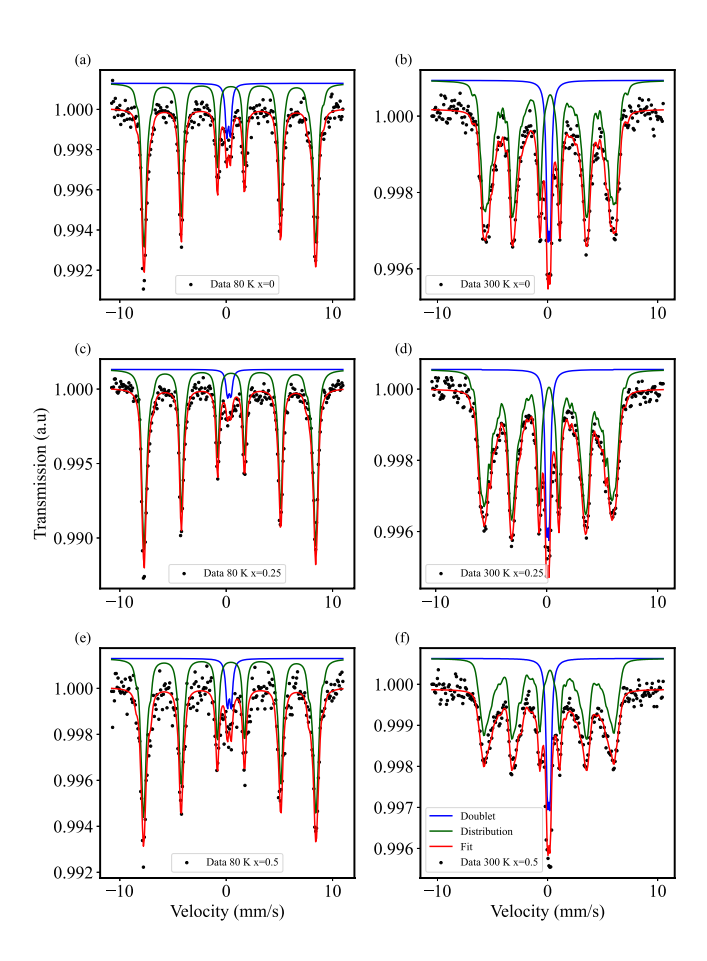


**Fig. 4.** Mössbauer spectra for  $GdBa_{1-x}Sr_xCuFeO_5$  x=0 at measured at 80 K (a) and 300 K (b), x=0.25 at 80 K (c) and 300 K (d), and x=0.5 at 80 K (e) and 300 K (f). Experimental data is represented by black dots, blue lines represent the fitted doublets, green lines represent magnetic distribution and total fits are represented by red lines.

spectra the same analysis was performed, but additional values of  $\delta$ ,  $\Delta E_Q$  and A were necessary to fit the observed doublet. The Mössbauer spectra and best fits for  ${\rm YBa}_{1-x}{\rm Sr}_x{\rm CuFeO}_5$  are shown in Fig. 3(a)–(f), for  ${\rm GdBa}_{1-x}{\rm Sr}_x{\rm CuFeO}_5$  in 4(a)–(f), the respective  $B_{hf}$  distributions are shown in Figs. 5 and 6, and all the corresponding hyperfine parameters are shown in Tables 3 and 4.

The effect of Sr doping at the Ba site in YBa $_{1-x}$ Sr $_x$ CuFeO $_5$  and GdBa $_{1-x}$ Sr $_x$ CuFeO $_5$  is reflected in the behavior of the hyperfine parameters displayed in Table 3. A progressive reduction of  $\delta$  with x for each temperature is attributed to the effect of a positive chemical pressure leading to a reduction of the cell volume [28]. Besides,  $\delta$  values for both temperatures are indicative of a Fe $^{3+}$  valence state for Fe.

The magnetic hyperfine field distributions extracted from the fits for YBa<sub>1-x</sub>Sr<sub>x</sub>CuFeO<sub>5</sub> and GdBa<sub>1-x</sub>Sr<sub>x</sub>CuFeO<sub>5</sub> are shown in Figs. 5 and 6, respectively, and the corresponding average hyperfine fields  $B_{hf}$  for each spectrum are presented in Table 3. It is seen that for YBaCuFeO<sub>5</sub> the magnetic hyperfine field distribution shape and average values ( $\overline{B_{hf}}$ is 36(7) T) are similar to others reported previously [14-16]. Similar results are obtained for  $GdBa_{1-x}Sr_xCuFeO_5$  (see Table 3). The large range of hyperfine field values seen in their distributions at 300 K are mainly due to the proximity of  $T_{N1}$  to the temperature in which the spectra were obtained, and variations in the Fe local environment or spin fluctuations persisting below  $T_{N1}$  may be responsible for volumes in the sample with smaller hyperfine fields [15]. At 80 K, the spectra for the YBa<sub>1-x</sub>Sr<sub>x</sub>CuFeO<sub>5</sub> and GdBa<sub>1-x</sub>Sr<sub>x</sub>CuFeO<sub>5</sub> show reduced line broadening (Figs. 3 and 4), nevertheless, the magnetic hyperfine field distributions in Figs. 5 and 6 show well defined peaks, and the estimated  $\overline{B_{hf}}$  values are close to those previously reported [14– 16]. Also,  $\overline{B_{hf}}$  shows a decrease with Sr doping for both sets of samples at 300 K, which suggests that Sr doping may be causing a decrease in  $T_{N1}$ , in agreement with a reduction of  $T_{N1}$  upon Sr doping previously reported [11]. The angle  $\theta$  between  $B_{hf}$  and  $V_{zz}$  is also reported in Table 3. At 300 K, the value of  $\theta$  increases with Sr doping for  $YBa_{1-x}Sr_xCuFeO_5$  while, at 80 K,  $B_{hf}$  remains aligned nearly perpendicular to the c-axis. The average quadrupole splitting  $\overline{\Delta E_O}$  is estimated from the correlation between  $B_{hf}$  and  $\Delta E_{O}$  through a linear dependence of the form  $\Delta E_Q = a + bB_{hf}$ ; the obtained values for a and bare shown in Table 4. These values imply that Fe sites with lower local disorder caused by differences in the local charge distribution will have larger magnetic hyperfine fields. This is reasonable if we consider that Fe-Fe pairs will introduce frustration in the lattice by minor differences and will have the largest exchange interactions [11]; the replacement of Fe atoms by Cu near a Fe site will reduce the local field and enhance the electrostatic distortion. Furthermore, this is qualitatively consistent with EFG calculations reported previously [16], however, our method is limited because it does not allow negative values of  $\Delta E_O$  and relies strongly on the hypothesis that the linear relation between  $B_{hf}$  and  $\Delta E_Q$  is valid.

For comparison with previous studies, the quadrupole shift  $2\varepsilon=\frac{\Delta E_Q}{2}\left(\frac{3\cos^2\theta-1}{2}\right)$  was calculated with the values obtained for  $\Delta E_Q$  and  $\theta$ , and is also reported for all the spectra in Table 3; the corresponding uncertainties were estimated through error propagation of the uncertainty of  $\overline{\Delta E_Q}$ . The  $\overline{\Delta E_Q}$  and  $2\varepsilon$  values at 300 K for YBa $_{1-x}$ Sr $_x$ CuFeO $_5$ 

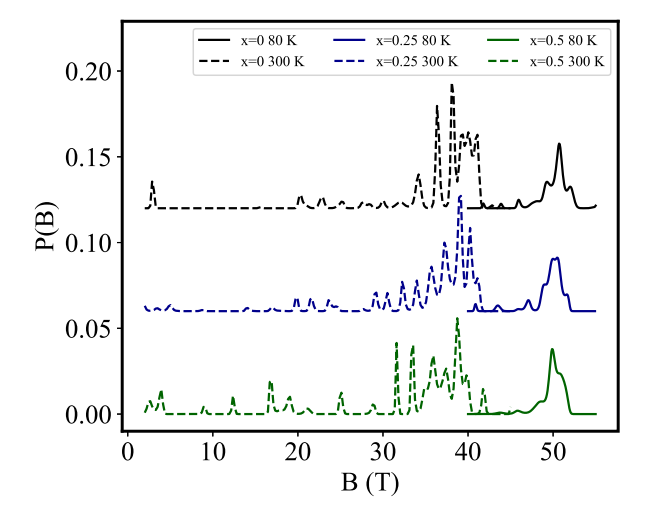


Fig. 5. Magnetic hyperfine field distributions for  $YBa_{1-x}Sr_xCuFeO_5$  (x=0,0.25,0.5) at 80 K and 300 K.

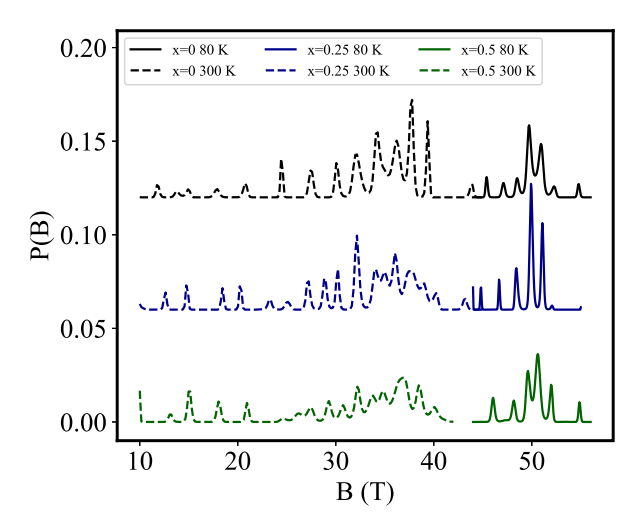
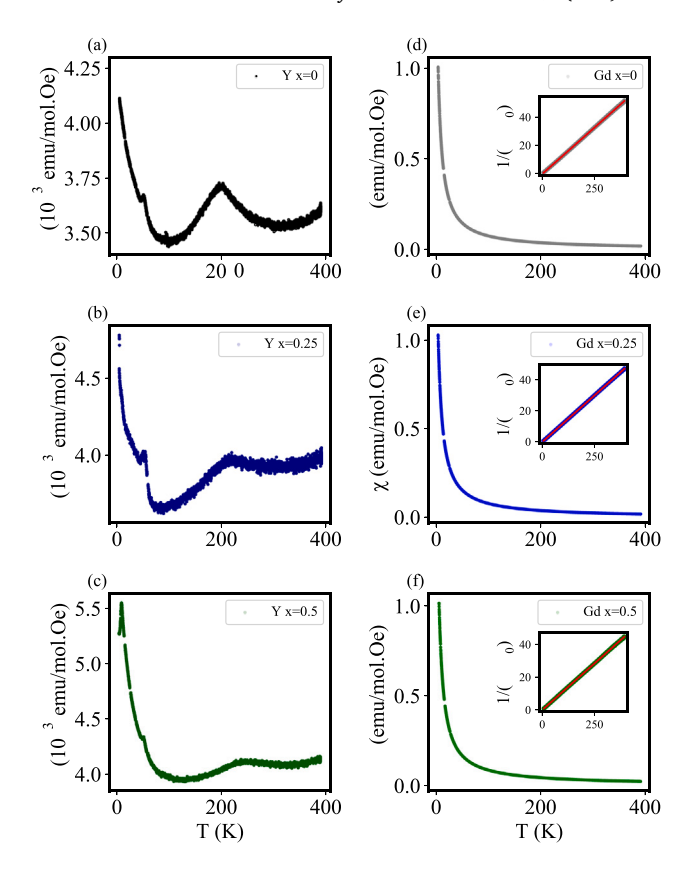


Fig. 6. Magnetic hyperfine field distributions for  ${\rm GdBa_{1-x}Sr_xCuFeO_5}$  (x=0,0.25,0.5) at 80 K and 300 K.

**Table 4** Correlation parameters a and b from the linear equation  $\Delta E_Q = a + bB_{hf}$  employed as correlation function between the hyperfine parameters obtained from the  $B_{hf}$  distributions extracted from the fits of Mössbauer spectra of  $YBa_{1-x}Sr_xCuFeO_5$  and  $GdBa_x$ . Sr  $CuFeO_x$  shown in Figs. 5 and 6.

Guba <sub>1-x</sub> 51 <sub>x</sub> GurcO <sub>5</sub> , shown in 11gs. 5 and 6.					
Sample	T (K)	a (mm/s)	b (mm/sT)		
$\mathbf{Y} \ x = 0$	300	0.87(6)	-0.014(4)		
$\mathbf{Y} \ x = 0$	80	0.65(1)	-0.010(1)		
Y x = 0.25	300	0.84(6)	-0.017(4)		
Y x = 0.25	80	0.81(1)	-0.013(1)		
Y $x = 0.5$	300	0.81(5)	-0.016(4)		
Y $x = 0.5$	80	0.78(1)	-0.011(1)		
Gd x = 0	300	0.59(5)	-0.014(4)		
Gd x = 0	80	0.82(1)	-0.011(1)		
Gd $x = 0.25$	300	0.65(5)	-0.013(4)		
Gd $x = 0.25$	80	0.76(1)	-0.010(1)		
Gd $x = 0.5$	300	0.56(5)	-0.011(4)		
Gd $x = 0.5$	80	0.74(1)	-0.009(1)		

are consistent with those reported previously [14–16], however, the large error bars (around 50%) do not allow any conclusion about the Sr doping effect; for  $GdBa_{1-x}Sr_xCuFeO_5$  an increase in  $\overline{\Delta E_Q}$  and  $2\varepsilon$  is more clearly seen upon Sr doping. This can be associated to



**Fig. 7.** Temperature dependence of the magnetic susceptibility measured for  $YBa_{1-x}Sr_xCuFeO_5$  (a–c) and  $GdBa_{1-x}Sr_xCuFeO_5$  (d–f). The insets at (d–f) show  $\frac{1}{\chi-\chi_0}$  and their respective fit (red line). The external field employed for all the measurements is 1 kOe.

the degree of lattice inhomogeneities at the Fe sites caused by the enhanced Fe/Cu disorder combined with the intrinsic inhomogeneity caused to the crystal lattice by a smaller Sr ion at the Ba site. At 80 K,  $\overline{AE_Q}$  and  $2\epsilon$  show smaller variations between them upon doping, but there is a marked difference between the values for YBa $_{1-x}$ Sr $_x$ CuFeO $_5$  and GdBa $_{1-x}$ Sr $_x$ CuFeO $_5$ : an increase of the quadrupole values may be influenced by the chemical compression of the lattice, leading to further deformation of the electric Fe surroundings and increasing the electric field gradient at the Fe site.

For the  ${\rm GdBa_{1-x}Sr_xCuFeO_5}$  is observed the presence of a paramagnetic doublet in all spectra, with  $\delta$  and  $\Delta E_Q$  values smaller and larger than the major phase, respectively. Also, according to the evolution of the resonance area, its cause can be attributed to small volumes of the sample with high local disorder or Fe/Cu clustering that may have lower transition temperatures. This volume separation can be unseen in techniques such as neutron diffraction, that has been largely and successfully employed in the study of the influence of the Fe/Cu site disorder, the q-vector incommensurability, and the increase in  $T_{N2}$  [7,11,17].

### 3.3. Magnetization

Temperature-dependence of magnetic susceptibility measurements between 2–380 K for  $YBa_{1-x}Sr_xCuFeO_5$  and  $GdBa_{1-x}Sr_xCuFeO_5$  are shown in Fig. 7(a-f). Remarkable differences between the  $YBa_{1-x}Sr_xCuFeO_5$  and the  $GdBa_{1-x}Sr_xCuFeO_5$  are seen: the observation of broad peaks between 200–250 K related to  $T_{N2}$  for the  $YBa_{1-x}Sr_xCuFeO_5$  contrasting with the paramagnetic behavior of the  $GdBa_{1-x}Sr_xCuFeO_5$ , a three-order of magnitude difference in the magnetic susceptibility at low temperatures, as well as the absence of any signature of magnetic transitions for  $GdBa_{1-x}Sr_xCuFeO_5$ , as reported previously [11].

A shift of  $T_{N2}$  towards higher temperatures with Sr doping is observed for the YBa<sub>1-x</sub>Sr<sub>x</sub>CuFeO<sub>5</sub>, starting from  $T_{N2} \simeq 200$  K at x=0 to  $T_{N2} \simeq 245$  K at x=0.5 (Fig. 7(a)–(c)). This shift was expected, being attributed to the effect of disorder induced by the Sr at the Ba site [11,23]. Furthermore, there is an enhanced response at lower temperatures for the YBa<sub>1-x</sub>Sr<sub>x</sub>CuFeO<sub>5</sub> that may be related to the possible mixture of magnetic phases reported previously. Also, the maximum in the susceptibility at  $T_{N2}$  broadens because of the disorder caused by the Sr doping. In addition, a feature is observed around 50 K, associated to the paramagnetic response of a small fraction of oxygen trapped in the sample holder. For YBa<sub>0.5</sub>Sr<sub>0.5</sub>CuFeO<sub>5</sub>, a third transition is observed close to 10 K, whose origin may be attributed to the onset of a different magnetic phase [11].

Regarding the behavior of the GdBa $_{1-x}$ Sr $_x$ CuFeO $_5$ , we observed a dominant paramagnetic response for all the samples, suggesting that the Gd moments are responsible for the macroscopic magnetic behavior. The temperature-independent susceptibilities  $\chi_0$  for GdBa $_{1-x}$ Sr $_x$ CuFeO $_5$  with x=0,0.25,0.5 are 0.004(1), 0.002(1) and 0.003(1) emu/mol·Oe, respectively; the effective magnetic moments  $\mu_{eff}$  are 7.78(1), 8.15(1) and 8.39(1) $\mu_B$ , all values relatively close to the free ion value expected for Gd of 7.94  $\mu_B$ ; and the Curie–Weiss temperatures are -1.07(2), -2.69(1) and -3.68(2) K, confirming the paramagnetic behavior observed. The Fe and Cu magnetic moments do not contribute to the paramagnetic effective moment because they are already ordered, as confirmed by Mössbauer experiments.

The absence of any further transitions explored by  $\frac{d(1/\chi)}{dT}$  and  $\chi_{AC}$  (not shown) implies that, within that sensitivity allowed by the technique, the  $GdBa_{1-x}Sr_xCuFeO_5$  are paramagnetic. However, from Mössbauer spectroscopy we confirm a magnetic state. This discrepancy can be explained if the Gd moments are considered as non-interacting with the Fe/Cu magnetic lattice due to the oxygen vacancies in the structure that suppress possible forms to enable a superexchange interaction between Gd and Fe/Cu, as in the simple rare-earth perovskites [34–38].

#### 4. Discussion

The effect caused in the crystal structure by doping on the YBa $_{1-x}$ Sr $_x$ CuFeO $_5$  and GdBa $_{1-x}$ Sr $_x$ CuFeO $_5$  is reflected in the line shift observed by FTIR, where it has been found that the effect of Sr doping affects mostly the apical oxygen dynamics. On the other hand, Mössbauer spectroscopy reflect the chemical doping effect on  $\delta$  and  $\Delta E_Q$ . In particular for  $\Delta E_Q$ , an increase at low temperatures upon doping can be associated to a distortion of the Fe/Cu bipyramids caused by the positive chemical effect induced by Sr doping. We see a similar behavior when replacing Y by Gd. These effects have been addressed as well by techniques such as synchrotron/neutron diffraction [11,17,39], and our expectation is that it would also be possible to relate further changes in parameters such as wavenumber shift, isomer shift or quadrupole interaction with site disorder at the Fe/Cu site, but a thorough analysis will be necessary.

Evidence for site disorder is also extracted from the increase in FTIR wavenumber and  $\Delta E_Q$  widths, which is ultimately related to the distributions of  $B_{hf}$  extracted from the fits. At 300 K, the distributions shown in Figs. 5 and 6 reflect that, upon Sr doping, the number of peaks and their heights for small hyperfine fields increase. The resonance areas of the paramagnetic site observed in Fig. 4 also increase with Sr-doping. At 80 K, closer to the saturation of  $B_{hf}$  [15], both the distribution peaks and the paramagnetic areas are reduced, suggesting that longrange magnetic order is causing  $B_{hf}$  to have a sharper distribution, probably because of long-range magnetic interactions and reduced spin fluctuations that are not strongly affected by thermal fluctuations at this temperature. It is worth mentioning that, at 80 K, Figs. 5 and 6 clearly show at least 4 peaks that, within our model, could be associated to different Fe site environments; the larger the  $B_{hf}$  the smaller the  $\Delta E_Q$  for that site, and thus a Fe site with large  $B_{hf}$  would correspond to a

less distorted site by the Fe/Cu occupancies, i.e. a Fe site surrounded by Fe atoms.

While the Sr-doping effect on the  $YBa_{1-x}Sr_xCuFeO_5$  is clear from FTIR, Mössbauer spectroscopy and magnetization, the corresponding effect in the magnetization for  $GdBa_{1-x}Sr_xCuFeO_5$  is barely seen, where a paramagnetic response is observed. As previously reported [11], rare-earth atom substitution at the Y site in YBaCuFeO<sub>5</sub> enables the control of Fe/Cu site disorder and the crystal structure, while no apparent signature of the spiral ordering temperature could be observed. This is compatible with the Mössbauer spectra, where sextets indicative of a hyperfine field at the Fe site confirm magnetic order, despite the paramagnetic behavior in the magnetization (Fig. 7).

In rare-earth perovskites, it is observed the effect of RE-Fe moment coupling and magnetic transitions at low temperatures attributed to rare-earths [34–38]. Thus, the absence of such behavior in REBaCuFeO $_5$  may be attributed to the differences between the perovskite structure and that of YBaCuFeO $_5$ , where the oxygen missing from the structure leads to the characteristic bipyramid scheme. The Fe/Cu site disorder effects on the magnetic properties of doped-YBaCuFeO $_5$  should be better observed using non-magnetic elements such as Sc, Lu or La, although La is known to be stable in an orthorhombic structure and showing magnetic order below room temperature [33,40]. Further systematic studies on how doping affect locally the Fe surroundings would also be desirable. Also, the ferroelectricity of the samples studied in this work is yet to be confirmed.

#### 5. Conclusions

The Fe/Cu site disorder in YBaCuFeO $_5$  either by Sr-doping at the Ba site or by replacing Y by Gd was studied by FTIR, Mössbauer spectroscopy and magnetization measurements. The chemical substitutions affect mostly the bipyramids along the c-axis, and the degree of Fe/Cu site disorder affects directly the magnetic properties, as reflected by the behavior of  $B_{hf}$  extracted from Mössbauer analysis. The replacement of Y by Gd only affects the crystal structure and the Fe/Cu disorder, while the Gd magnetic moment apparently has no interplay with the Fe/Cu magnetic moments.

# CRediT authorship contribution statement

I.M. Saavedra-Gaona: Methodology, Investigation, Data curation. F. Mesquita: Methodology, Investigation, Formal analysis, Data curation. R. Cohen: Data curation. L.C.C.M. Nagamine: Writing – review & editing, Methodology, Investigation. C.A. Parra-Vargas: Writing – review & editing, Investigation, Funding acquisition, Conceptualization. J. Munevar: Writing – original draft, Visualization, Methodology, Funding acquisition, Formal analysis, Data curation, Conceptualization.

## **Declaration of competing interest**

The authors declare the following financial interests/personal relationships which may be considered as potential competing interests: Julian Munevar reports financial support was provided by State of Sao Paulo Research Foundation. Julian Munevar reports administrative support was provided by Federal University of the ABC. If there are other authors, they declare that they have no known competing financial interests or personal relationships that could have appeared to influence the work reported in this paper.

### Data availability

Data will be made available on request.

# Acknowledgments

This work was supported by FAPESP (Grant No. 2017/20989-8). We are thankful to the UFABC CEM for providing access to its experimental facilities.

#### References

- [1] D. Khomskii, Classifying multiferroics: Mechanisms and effects, Physics 2 (2009)
- [2] M. Fiebig, T. Lottermoser, D. Meier, M. Trassin, The evolution of multiferroics, Nat. Rev. Mater. 1 (2016) 16046.
- [3] J. Wang, J.B. Neaton, H. Zheng, V. Nagarajan, S.B. Ogale, B. Liu, D. Viehland, V. Vaithyanathan, D.G. Schlom, U.V. Waghmare, N.A. Spaldin, K.M. Rabe, M. Wuttig, R. Ramesh, Expitaxial BiFeO<sub>3</sub> multiferroic thin film heterostructures, Science 299 (2003) 1719.
- [4] T. Kimura, T. Goto, H. Shintani, K. Ishizaka, T. Arima, Y. Tokura, Magnetic control of ferroelectric polarization, Nature 426 (2003) 55–58.
- [5] Y. Kawamura, T. Kai, E. Satomi, Y. Yasui, Y. Kobayashi, M. Sato, K. Kakurai, High-temperature multiferroic state of RBaCuFeO<sub>5</sub> (R=Y,Lu, and Tm), J. Phys. Soc. Japan 79 (7) (2010) 073705.
- [6] M. Morin, A. Scaramucci, M. Bartkowiak, E. Pomjakushina, G. Deng, D. Sheptyakov, L. Keller, J. Rodríguez-Carvajal, N.A. Spaldin, M. Kenzelmann, K. Conder, M. Medarde, Incommensurate magnetic structure, Fe/Cu chemical disorder, and magnetic interactions in the high-temperature multiferroic YBaCuFeO<sub>5</sub>, Phys. Rev. B 91 (2015) 064408.
- [7] M. Morin, E. Canévet, A. Raynaud, M. Bartkowiak, D. Sheptyakov, V. Ban, M. Kenzelmann, E. Pomjakushina, K. Conder, M. Medarde, Tuning magnetic spirals beyond room temperature with chemical disorder, Nature Commun. 7 (2016) 13758.
- [8] Y.C. Lai, C.H. Du, C.H. Lai, Y.H. Liang, C.W. Wang, K.C. Rule, H.C. Wu, H.D. Yang, W.T. Chen, G.J. Shu, F.C. Chou, Magnetic ordering and dielectric relaxation in the double perovskite YBaCuFeO<sub>5</sub>, J. Phys.: Condens. Matter. 29 (2017) 145801.
- [9] S. Lal, S.K. Upadhyay, L. Mukherjee, C.S. Yadav, Evolution of magnetic and dielectric properties in sr-substituted high-temperature multiferroic YBaCuFeO<sub>5</sub>, Europhys. Lett. 117 (2017) 67006.
- [10] S. Luo, K. Wang, Giant dielectric permitivity and magneto-capacitance effect in YBaCuFeO<sub>5</sub>, Scr. Mater. 146 (2018) 160–163.
- [11] T. Shang, E. Canévet, M. Morin, D. Sheptyakov, M.T. Fernández-Díaz, E. Pomjakushina, M. Medarde, Design of magnetic spirals in layered perovskites: extending the stability range far beyond room temperature, Sci. Adv. 4 (2018) 42316386
- [12] H.W. Chen, Y.W. Chen, J.L. Kuo, Y.C. Lai, F.C. Chou, C.H. Du, H.L. Liu, Spin-charge-lattice coupling in YBaCuFeO<sub>5</sub>: optical properties and first-principles calculations, Sci. Rep. 9 (2019) 3223.
- [13] X. Zhang, A. Romaguera, O. Fabelo, F. Fauth, J. Herrero-Martín, J.L. García-Muñoz, Tuning the tilting of the spiral plane by Mn doping in YBaCuFeO<sub>5</sub> multiferroic, Acta Mater. 206 (2021) 166608.
- [14] L. Er-Rakho, C. Michel, Ph. Lacorre, B. Raveau, YBaCuFeO $_{5+\delta}$ : a novel oxygen-deficient perovskite with a layer structure, J. Solid State Chem. 73 (1988) 531–535
- [15] C. Meyer, F. Hartmann-Boutron, Y. Gros, P. Strobel, Mössbauer study of YBaCuFeO $_{5+\delta}$ : site assignments of the metallic ions, Solid State Commun. 76 (1990) 163–168.
- [16] V. Caignaert, I. Mirebeau, F. Bourée, N. Nguyen, A. Ducouret, J.-M. Greneche, B. Raveau, Crystal and magnetic structure of YBaCuFeO<sub>5</sub>, J. Solid State Chem. 114 (1995) 24–35.
- [17] A. Romaguera, X. Zhang, O. Fabelo, F. Fauth, J. Blasco, J.L. García-Muñoz, Helimagnets by disorder: its role on the high-temperature magnetic spiral in the YBaCuFeO<sub>5</sub> perovskite, Phys. Rev. Res. 4 (2022) 043188.
- [18] Y.K. Atanassova, V.N. Popov, G.G. Bogachev, M.N. Iliev, Raman- and infraredactive phonons in YBaCuFeO<sub>5</sub>: experiment and lattice dynamics, Phys. Rev. B 47 (1993) 15201
- [19] B. Kundys, A. Maignan, Ch. Simon, Multiferroicity with high- $T_C$  in ceramics of the YBaCuFeO<sub>5</sub> ordered perovskite, App. Phys. Lett. 94 (2009) 072506.
- [20] M.J. Ruiz-Aragón, E. Morán, R. Sáez-Puche, N. Menéndez, J.D. Tornero, Antiferromagnetic interactions and Mössbauer study of LnMCuFeO<sub>5+δ</sub> phases (Ln=Y,La; M=Ca,Sr,Ba)), J. Superconductivity 9 (2) (1996) 155–160.

- [21] A. Scaramucci, H. Shinaoka, M.V. Mostovoy, M. Müller, C. Mudry, M. Troyer, N.A. Spaldin, Multiferroic magnetic spirals induced by random magnetic exchanges, Phys. Rev. X 8 (2018) 011005.
- [22] A. Scaramucci, H. Shinaoka, M.V. Mostovoy, R. Lin, C. Mudry, M. Müller, Spiral order from orientationally correlated random bonds in classical XY models, Phys. Rev. Res. 2 (2020) 013273.
- [23] V. Porée, D.J. Gawryluk, T. Shang, J.A. Rodríguez-Velamazán, N. Casati, D. Sheptyakov, X. Torrelles, M. Medarde, Yba<sub>1-x</sub>Sr<sub>x</sub>CuFeO<sub>5</sub> layered perovskites: exploring the magnetic order beyond the paramagnetic-collinear-spiral triple point, 2024, arXiv:2402.04816.
- [24] D. Dey, S. Nandy, T. Maitra, C.S. Yadav, A. Taraphder, Nature of spiral state and absence of electric polarisation in Sr-doped YBaCuFeO<sub>5</sub> revealed by first-principle study. Sci. Rep. 8 (2018) 2404.
- [25] S. Lal, K. Mukherjee, C.S. Yadav, Thermal conductivity of multiferroic material YBa<sub>1-x</sub>Sr<sub>x</sub>CuFeO<sub>5</sub> (x = 0, 0.25, 0.5), in: AIP Conf. Proceedings 2005, 2018, 050001.
- [26] M.J. Ruiz-Aragón, E. Morán, U. Amador, J.L. Martínez, N.H. Andersen, H. Ehrenberg, Low-temperature magnetic structure of YBaCuFeO<sub>5</sub> and the effect of partial substitution of yttrium by calcium, Phys. Rev. B 58 (1998) 6291.
- [27] S. Lal, K. Mukherjee, C.S. Yadav, Effect of crystalline electric field on heat capacity in LnBaCuFeO<sub>5</sub> (Ln=Gd, Ho, Yb), Solid State Commun. 270 (2018) 130–134.
- [28] I.M. Saavedra Gaona, J. Munevar, C.A. Parra Vargas, Evaluation of rare earth substitution in the structural and magnetic properties of the  $REBa_{1-x}Sr_xCuFeO_{5+\delta}$  and  $YbBa_{1-x}Sr_xCuFeO_{5+\delta}$  (x=0,0.25,0.5) ceramic systems, Mater. Sci. Eng. B 280 (2022) 115719.
- [29] S. Kamusella, H.H. Klauss, Moessfit, Hyperfine Interact. 237 (1) (2016) 1-10.
- [30] A.I. Klyndyuk, E.A. Chizhova, Structure and electrical and transport properties of cation-deficient samples of perovskite ferrocuprates RBaCuFeO<sub>5+5</sub> (R= Y, La), PhSS 50 (4) (2008) 603–608, http://dx.doi.org/10.1134/S1063783408040021.
- [31] A. Klyndyuk, Oxide thermoelectrics view project oxide multiferroics view project layered perovskite-like oxides 0112 type: Structure, properties, and possible applications, ChemInform 42 (2011) 59–105.
- [32] N. Nazir, A. Ikram, M. Ikram, Impact of a non-magnetic  $Sr^{2+}$  ion doping on the magnetic and optical properties of  $Gd_{2-x}Sr_xNiMnO_6$  (x=0,0.3,0.5) double perovskite, J. Magnet. Magnet. Mater. 571 (2023) 170549.
- [33] A.L. Ben Hafsia, N. Rammeh, M. Ferid, N. Errien, J.M. Greneche, M. Khitouni, Alternative current conduction, dielectric behavior, transport properties and Mössbauer study of LaBaFe<sub>0.5</sub>Ti<sub>0.5</sub>MnO<sub>6-δ</sub> new compound, J. Alloys Comp. 695 (2017) 3310–3317.
- [34] G.W. Durbin, C.E. Johnson, M.F. Thomas, Temperature dependence of field-induced spin reorientation in GdFeO<sub>3</sub>, J. Phys. C: Solid State Phys. 10 (1976) 1975–1978
- [35] P. Paul, C.L. Prajapat, A.K. Rajarajan, T.V. Chandrasekar Rao, Low temperature magnetic properties of GdFeO<sub>3</sub>, AIP Conf. Proc. 1942 (2018) 130029.
- [36] A. Panchwanee, S.K. Upadhyay, N.P. Lalla, V.G. Sathe, A. Gupta, V. Raghavendra Reddy, Low-temperature Raman, high magnetic field<sup>57</sup>Fe Mössbauer, and x-ray diffraction study of magnetodielectric coupling in polycrystalline GdFeO<sub>3</sub>, Phys. Rev. B 99 (2019) 064433.
- [37] K.A. Shaykhutdinov, S.A. Skorobogatov, Yu.V. Knyzaev, T.N. Kamkova, A.D. Vasiljev, S.V. Semenov, M.S. Pavlovskii, A.A. Krasikov, Controlling the temperature of the spin-reorientation transition in HoFe<sub>1-x</sub>Mn-xO<sub>3</sub> orthoferrite single crystals, 2023, arXiv:2307.08236.
- [38] F. Bzour, I.Z. Al-Yahmadi, A. Gismelseed, F. Al Ma'Mari, O. Cespedes, A. Al-Rawas, H. Widatallah, Crystal structure magnetic and Mössbauer studies of DyFe $_x$ Mn $_{1-x}$ O-3 multiferroic magnanites, Physica B 673 (2024) 415507.
- [39] A. Romaguera, X. Zhang, R. Li, O. Fabelo, J.L. García-Muñoz, Magnetic properties of highly ordered single crystals with layered YBaCuFeO<sub>5</sub> structure, EPJ Web Conf. 286 (2023) 05005.
- [40] I.M. Saavedra Gaona, E. Moncada-Villa, C.A. Ortiz-Otálora, J. Munevar, C.A. Parra Vargas, Structural and magnetic properties of LaBa<sub>1-x</sub>Sr<sub>x</sub>CuFeO<sub>5+ $\delta$ </sub> and YbBa<sub>1-x</sub>Sr<sub>x</sub>CuFeO<sub>5+ $\delta$ </sub> (x=0,0.25,0.5) ceramic systems, Mater. Charact. 191 (2022) 112079